

SEMANTICALLY AWARE UAV LANDING SITE ASSESSMENT FROM REMOTE SENSING IMAGERY VIA MULTIMODAL LARGE LANGUAGE MODELS

Chunliang HUA¹, Zeyuan YANG², Lei ZHANG², Jiayang SUN²,
Fengwen CHEN², Chunlan ZENG³, Xiao HU^{2†}

¹: School of Information Science and Engineering, Southeast University, Nanjing 211189, China

²: LASER, International Digital Economy Academy, Shenzhen 510085, China

³: Department of Electronic Engineering, East China Normal University, Shanghai 200241, China

ABSTRACT

Safe UAV emergency landing requires more than just identifying flat terrain; it demands understanding complex semantic risks (e.g., crowds, temporary structures) invisible to traditional geometric sensors. In this paper, we propose a novel framework leveraging Remote Sensing (RS) imagery and Multimodal Large Language Models (MLLMs) for global context-aware landing site assessment. Unlike local geometric methods, our approach employs a coarse-to-fine pipeline: first, a lightweight semantic segmentation module efficiently pre-screens candidate areas; second, a vision-language reasoning agent fuses visual features with Point-of-Interest (POI) data to detect subtle hazards. To validate this approach, we construct and release the **Emergency Landing Site Selection (ELSS)** benchmark. Experiments demonstrate that our framework significantly outperforms geometric baselines in risk identification accuracy. Furthermore, qualitative results confirm its ability to generate human-like, interpretable justifications, enhancing trust in automated decision-making. The benchmark dataset is publicly accessible at <https://anonymous.4open.science/r/ELSS-dataset-43D7>.

Index Terms— multimodal large language models, unmanned aerial vehicles, autonomous emergency landing, semantic segmentation

1. INTRODUCTION

Ensuring safety during emergency landings is a critical challenge for Uncrewed Aerial Vehicles (UAVs), particularly in complex urban environments where mechanical failures can lead to catastrophic ground collisions [1, 2]. Existing solutions primarily rely on geometric evaluation using onboard sensors, such as LiDAR or depth cameras, to identify flat surfaces for landing. These morphology-based methods [3–6] assess suitability by quantifying slopes and roughness from digital elevation models (DEMs) or point clouds [7–10].

This work was done when Chunliang Hua interns at IDEA.

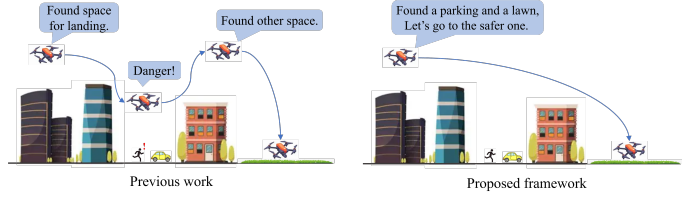


Fig. 1: Conceptual comparison between conventional geometry-based approaches and the proposed MLLM-driven framework for emergency landing site selection.

While effective for local obstacle avoidance, they fundamentally lack **semantic awareness**. In real-world scenarios, geometric flatness does not equate to safety; a flat lawn may be crowded with people, and a smooth parking lot may be an active traffic zone. These “semantic risks” are invisible to depth sensors but are critical for safe decision-making.

To bridge this gap, recent research in Remote Sensing (RS) has leveraged deep learning for semantic understanding. While domain-specific models like RSGPT [11], GeoChat [12], and EarthGPT [13] demonstrate that terrain semantics significantly enhance interpretation beyond elevation data, applying them to safety-critical landing tasks remains underexplored. Recent frameworks such as Flight-GPT [14] and LLM-Land [15] have attempted to use MLLMs for context-aware decisions. However, these approaches often prioritize general autonomy over strict safety compliance (e.g., JARUS SORA guidelines [16]), and they typically lack the explainability required for high-stakes operations.

In this paper, we propose a novel **Semantic Risk Assessment Framework** that leverages RS imagery and MLLMs to identify safe landing sites from a global perspective. Unlike resource-constrained onboard processing, our approach utilizes satellite imagery for macro-scale analysis, serving as a high-level decision support system. We introduce a *coarse-to-fine* pipeline: first, a semantic segmentation module filters out obvious non-landable areas; second, a vision-language reasoning agent evaluates candidate sites by fusing visual fea-

tures with Point-of-Interest (POI) data. This allows the system to not only select safe sites but also provide **interpretable natural language justifications** for its decisions.

The main contributions of this work are summarized as follows: 1) We propose the first MLLM-driven framework for UAV landing site assessment, shifting the paradigm from purely geometric analysis to semantic understanding; 2) We construct and release the **Emergency Landing Site Selection (ELSS)** benchmark dataset¹, which contains diverse urban and rural scenarios with expert annotations to facilitate future research. Experimental results demonstrate that our method significantly outperforms geometric baselines in risk identification. Furthermore, qualitative analysis confirms that our model generates human-like explanations, enhancing the transparency and trustworthiness of the automated system.

The remainder of this paper is organized as follows: Section 2 details our three-stage pipeline; Section 3 presents experimental results; and Section 4 concludes with future directions.

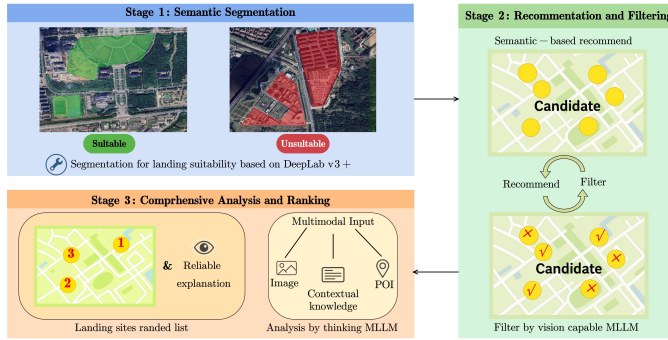


Fig. 2: Scheme chart of the proposed framework.

2. METHOD

The proposed framework, illustrated in Fig. 2, is structured as a coarse-to-fine pipeline designed to simulate human pilot cognition. It progressively filters landing candidates by integrating visual perception with semantic reasoning.

2.1. Problem Formulation

Let $\mathcal{I} \in \mathbb{R}^{H \times W \times 3}$ be the input remote sensing image and $\mathcal{P} = \{p_1, p_2, \dots, p_k\}$ be the set of nearby Point-of-Interest (POI) data. Our goal is to identify a ranked list of landing sites $\mathcal{S} = \{s_1, s_2, \dots, s_m\}$, where each site s_i is defined by a bounding box b_i , a safety score $\sigma_i \in [0, 1]$, and a natural language justification \mathcal{T}_i . The problem is modeled as a hierarchical filtering process:

$$\mathcal{S} = f_{\text{reason}}(f_{\text{verify}}(f_{\text{seg}}(\mathcal{I})), \mathcal{P}, \mathcal{C}_{\text{dyn}}) \quad (1)$$

where f_{seg} , f_{verify} , and f_{reason} correspond to the semantic segmentation, visual verification, and context reasoning modules, respectively, and \mathcal{C}_{dyn} represents dynamic context (e.g., time, weather).



Fig. 3: Comparison of remote sensing imagery and standard maps highlighting segmentation results. The figure shows correct segmentation of the upper forest half and misclassification of the lower half as background, emphasizing the limitations of using only satellite images for segmentation.

2.2. Stage 1: Semantic Filtering via Segmentation

The first stage aims to efficiently parse large-scale remote sensing imagery to generate a set of potential landing candidates, reducing the search space for the subsequent MLLM. We employ the DeepLabV3+ [17] framework (implemented via MMSegmentation [18]) due to its superior capability in handling scale variations inherent in aerial views. Unlike standard U-Net architectures, DeepLabV3+ utilizes Atrous Spatial Pyramid Pooling (ASPP) to capture multi-scale context without losing resolution. Mathematically, the atrous convolution for a signal x , filter w , and dilation rate r is defined as $y[i] = \sum_k x[i + r \cdot k] \cdot w[k]$. This mechanism allows the network to distinguish between large homogeneous regions (e.g., lakes) and fine-grained structures (e.g., narrow roads), which is critical for identifying safe landing zones.

However, deploying this model reveals significant *domain shift* challenges. While the network achieves high accuracy on high-resolution aerial datasets like ISPRS Potsdam [19], its performance degrades on lower-resolution satellite imagery (e.g., our Nanjing dataset, see Sec. 3). As illustrated in Fig. 3, differences in texture and spectral characteristics lead to systematic misclassifications, such as dense forests being labeled as soil due to texture smoothing. Relying solely on visual segmentation in such heterogeneous data sources risks proposing hazardous sites. To address these misclassification issues, a strategy was proposed, as described in Fig. 4, to cross-validate the classification results using map information. This flow chart illustrates the integration of a semantic segmentation network, $S(\cdot)$, with a classification head, $C(\cdot)$, to evaluate pixel-wise landing suitability. By leveraging standard maps, this method enhances the reliability of pixel classification and addresses domain adaptation challenges. Ultimately, the semantic output not only iden-

¹Dataset link to be added upon publication.

tifies potential candidate sites for further analysis but also enhances efficiency by acting as a crucial filtering step. This hybrid approach transforms the segmentation step from a deterministic classifier into a *high-recall candidate generator*, ensuring that only plausibly safe regions are passed to the MLLM for fine-grained verification.

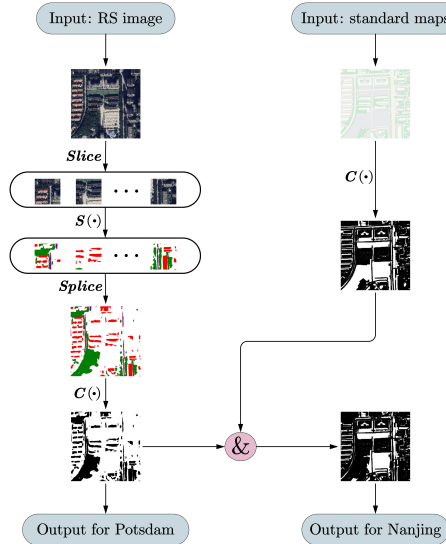


Fig. 4: The flow chart of proposed stage 1. Specifically, $S(\cdot)$ denotes the semantic segmentation network, and $C(\cdot)$ corresponds to the classification head that evaluates pixel-wise landing suitability.

2.3. Stage 2: Visual Verification via Iterative Proposals

While semantic segmentation offers a global view of land use, it lacks the fine-grained reasoning to distinguish between a “flat plaza” and a “cracked pavement.” To address this, we implement an iterative *propose-and-verify* loop (Fig. 5) that bridges pixel-level cues with high-level semantic reasoning.

The process begins by formalizing candidate generation as a spatial density search. We define a radially decaying convolution kernel K to identify centers of large, contiguous suitable regions. The kernel weights are designed to favor centrality:

$$K_{i,j} = 1 - \frac{(i-d)^2 + (j-d)^2}{2d^2}, \text{ for } i, j \in \{0, \dots, 2d\} \quad (2)$$

A response map is computed via $R = I * K$, where I is the binary suitability map from Stage 1. The location of the maximum response $(x^*, y^*) = \arg \max R(x, y)$ serves as the center for the current landing proposal. This convolution-based approach naturally filters out fragmented noise and prioritizes compact regions suitable for the UAV’s footprint.

Once a candidate is proposed, we crop the corresponding high-resolution image patch and query a vision-capable VLM

to detect hazards invisible to the segmentation model (e.g., vehicles, rubble). The model is instructed via a specific prompt: “*Inspect this satellite image patch. Is the surface smooth and free of dynamic obstacles or structural hazards? Answer [Safe/Unsafe] and provide a 1-sentence reason.*” Based on the VLM’s verdict, we employ a dual-strategy **Tabu Mechanism** to dynamically update the response map $R(x, y)$ for the next iteration:

- **Successful Filter (Hard Suppression):** If the site is confirmed as Safe, we zero out the local neighborhood \mathcal{N} to enforce diversity: $R'(x, y) = 0, \forall (x, y) \in \mathcal{N}(x^*, y^*)$.
- **Failed Filter (Soft Penalty):** If rejected (e.g., due to temporary occupancy), we apply a Gaussian decay penalty to discourage revisiting the exact spot while allowing valid candidates nearby:

$$R'(x, y) = R(x, y) \cdot \frac{(x - x^*)^2 + (y - y^*)^2}{2d^2}, \forall (x, y) \in \mathcal{N} \quad (3)$$

This feedback loop continues iteratively, adaptively guiding the search toward novel, high-quality candidates without exhaustive re-sampling.

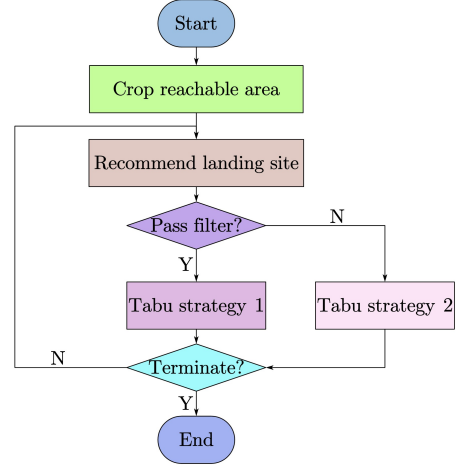


Fig. 5: Flow chart of the recommendation and filtering scheme.

2.4. Stage 3: Context-Aware Reasoning via Multi-Modal Fusion

The final stage mimics the high-level cognitive process of a human pilot, selecting the optimal landing site not just based on geometry, but on comprehensive safety protocols. We employ a reasoning-oriented MLLM to synthesize four heterogeneous information streams (Fig. 6):

- **Visual Evidence:** The high-resolution cropped patch of the candidate site passed from Stage 2.

- **Spatial Context (POI):** Static vector data retrieved from OpenStreetMap or Amap, quantifying proximity to sensitive facilities (e.g., schools, gas stations, power lines).
- **Dynamic Context:** Real-time environmental variables, including time of day, weather conditions, and active social events (e.g., “Rush Hour”, “Public Holiday”).
- **Regulatory Constraints:** A system prompt injecting domain-specific rules derived from JARUS SORA guidelines (e.g., “Maintain 1:1 buffer distance from people”).

By integrating these inputs, the MLLM performs *spatio-temporal reasoning*. For instance, it recognizes that a school playground, while visually flat (Safe geometrically), is a high-risk zone during weekdays at 10:00 AM (Unsafe semantically) but potentially viable at midnight. The model outputs a strictly ranked list of sites, where each recommendation is accompanied by a **Natural Language Justification** (e.g., “Rank 1: *Empty parking lot. Justification: Surface is flat, far from high-rise buildings, and currently outside of business hours with low dynamic risk.*”). This interpretability is crucial for auditability in safety-critical operations.

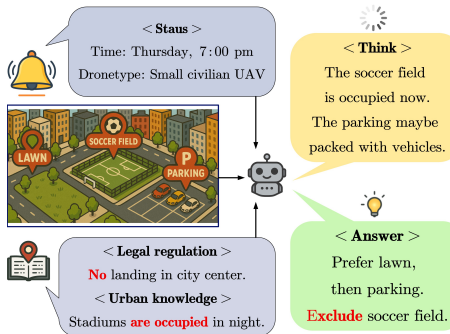


Fig. 6: Flowchart of the MLLM-driven comprehensive analysis stage, integrating remote sensing, POI, dynamic context, and domain knowledge for final site ranking.

3. EXPERIMENTAL RESULTS AND ANALYSIS

3.1. Study Area and Benchmarks

To evaluate the robustness of our framework across different sensor modalities, we utilize two distinct datasets representing contrasting regimes (Fig. 7):

- **ISPRS Potsdam (Airborne):** A high-resolution (0.05m/px) dataset depicting a dense German city. We utilize 20 tiles to create a $24,000 \times 30,000$ pixel composite. Segmentation is performed using a DeepLabV3+ model pretrained on Potsdam, treating *Background* and *Impervious Surfaces* as potential landing zones.

- **Nanjing (Satellite):** A custom dataset derived from Google Earth (0.3m/px), covering a diverse urban-rural fringe in China. Despite lower resolution, it spans $20 \times$ the area of Potsdam. We use a model pretrained on the LoveDA dataset [20] (which includes Nanjing samples) for domain adaptation, classifying *Background* and *Barren* as suitable.

The ELSS Benchmark: To standardize the evaluation of MLLM-based landing assessment, we constructed the **Emergency Landing Site Selection (ELSS)** benchmark. It consists of 500 expert-annotated samples (250 per region), where each sample includes the RS image patch, POI vector data, and a ground-truth safety label based on JARUS SORA guidelines.



(a) Potsdam (0.05m/px) (b) Nanjing (0.3m/px)

Fig. 7: Comparison of dataset domains. Potsdam represents high-res metrics, while Nanjing represents challenging low-res satellite scenarios.

Table 1: Efficiency of Candidate Generation: Comparison of “Passing Rate” (Percentage of candidates verified as Safe by MLLM) between Random Sampling and our Semantic Filtering.

MLLM Model	Potsdam		Nanjing	
	Random	Semantic	Random	Semantic
Qwen	34	50↑	74	89↑
Doubao	18	52↑	21	46↑
GPT-4.1	19	57↑	29	70↑

3.2. Model Behavior and Filtering Performance

We evaluated three MLLMs: Qwen-QVQ-max (Qwen), Doubao-Vision-Pro (Doubao), and GPT-4.1. Beyond the efficiency gains shown in Table 1, we analyzed the specific behavioral characteristics of each model to understand their suitability for safety-critical tasks. Across all models and both datasets, semantic-based recommendation consistently and significantly outperformed random sampling, demonstrating that early terrain classification effectively prunes unsuitable regions before costly MLLM inference. The improvement was most dramatic for GPT-4.1 on Potsdam, where the pass rate more than doubled from 19% to 57%.

The experiment also revealed notable differences in filtering strictness among the MLLM models. Doubao applied the most conservative criteria, exhibiting high reliability in detecting subtle hazards (e.g., cracks, vegetation density), even in complex scenes. Qwen, by contrast, was the most permissive, particularly on the Nanjing dataset, where it accepted 74% of randomly sampled sites. Further examinations of its responses revealed that this high pass rate was often due to misinterpretation of low-resolution or blurry imagery, leading to overconfident but inaccurate approvals. GPT-4.1 struck a balanced middle ground: robust visual understanding with moderate leniency, yielding stable performance across datasets. These qualitative distinctions reveal critical trade-offs in model selection: strictness improves safety but may reduce coverage; permissiveness increases availability at the cost of risk. The results underscore that MLLMs are not interchangeable in safety-critical applications—model choice must be aligned with operational constraints.

To rigorously quantify the quality of Stage 2 recommendations, we manually annotated semantic-based recommendations to quantitatively evaluate filter performance using precision (Prec.), recall (Rec.), and positive ratio (Pos. Rat.) that is the proportion of recommended sites deemed suitable by the MLLM. Results are summarized in [Table 2](#). The proportion of manually annotated positive samples was 57% (Potsdam) and 63% (Nanjing), representing the upper bound of true positives Stage 3 could receive without Stage 2’s filtering. This is significantly lower than the highest achieved precision rates of 90% and 85%, respectively, demonstrating that Stage 2 effectively eliminates false positives while preserving viable candidates. Comparative analysis across models further supports these findings: on Potsdam, both Doubao and GPT-4.1 achieved high and comparable precision and recall, indicating robust performance under favorable conditions. On the more challenging Nanjing dataset, Doubao prioritized precision (85%) at the cost of recall (62%), reflecting its conservative filtering strategy; in contrast, GPT-4.1 maintained a balanced trade-off (79% precision, 87% recall).

Table 2: Precision, recall, and positive ratio of the MLLM-based filter across datasets.

MLLM Model	Potsdam			Nanjing		
	Prec.	Rec.	Pos.	Prec.	Rec.	Pos.
			Rat.			Rat.
Qwen	82	72		66	94	
Doubao	90	82	57	85	62	63
GPT-4.1	86	86		79	87	

3.3. Ranking Performance and Ablation Study

To evaluate the final ranking stage, we constructed a curated benchmark of 200 queries. Each query contains four candi-

date sites with RS imagery and POI data, manually annotated for suitability. [Table 3](#) reports the *Right Rate* (R.R.) (correct identification of both best and worst sites), *False Rate* (F.R.) (critical ranking errors), and *Other* (no confident decision was made due to e.g. ambiguous context.).

Table 3: Ranking performance on the custom benchmark. (R.R.: Right Rate; F.R.: False Rate).

Method	Potsdam			Nanjing		
	R.R.	F.R.	Other	R.R.	F.R.	Other
Proposed Method	68%	11%	21%	67%	8%	25%
MLLM w/o POI	40% ¹²⁸	28%	32%	44% ¹²³	27%	29%
Random Baseline	11%	33%	56%	11%	33%	56%

Results & Ablation: The proposed framework achieves a consistent R.R. of $\approx 68\%$, significantly outperforming the random baseline (11%). Crucially, the ablation study (“w/o POI”) reveals that removing contextual data causes a sharp performance drop of **28%** on Potsdam and **23%** on Nanjing. This quantitatively proves that visual flatness alone is insufficient for safety; POI integration is essential to detect semantic hazards (e.g., schools, gas stations). Qualitative analysis suggests that the remaining errors primarily stem from subtle temporal ambiguities (e.g., specific opening hours), which represent current limits in MLLM reasoning rather than structural flaws in the pipeline. When excluding these 80 edge cases, the False Rate falls to just 5%, indicating that our system achieves high reliability under typical operational conditions.

4. CONCLUSION

In this work, we presented a novel MLLM-driven framework for UAV emergency landing site assessment, shifting the paradigm from geometric morphology to semantic risk understanding. By integrating a coarse-to-fine segmentation pipeline with a vision-language reasoning agent, our method effectively identifies semantic hazards (e.g., crowds, temporary structures) invisible to traditional sensors while minimizing computational overhead. Experiments on the proposed ELSS benchmark demonstrate that our approach significantly outperforms baselines in risk identification accuracy. Crucially, the framework generates human-like, natural language justifications, ensuring the transparency and auditability required for safety-critical operations.

Current limitations include the inference latency of cloud-based MLLMs and the reliance on third-party satellite imagery quality. Future work will focus on two key directions: (1) **Model Distillation**, compressing reasoning capabilities into lightweight, edge-optimized networks for offline onboard deployment; and (2) **Dynamic Fusion**, integrating real-time data feeds (e.g., live traffic, weather) to further enhance situational awareness in complex urban environments.

5. REFERENCES

- [1] J. D. Kenny, “26th joseph t. nall report,” Tech. Rep., Richard G. McSpadden, JR., 2017. [1](#)
- [2] Australian Transport Safety Bureau, “Engine failures and malfunctions in light aeroplanes 2009–2014,” Tech. Rep., Investigation number AR-2013-107, March 2016. [1](#)
- [3] Mayank Garg, Abhishek Kumar, and P.B. Sujit, “Terrain-based landing site selection and path planning for fixed-wing uavs,” in *2015 International Conference on Unmanned Aircraft Systems*, 2015, pp. 246–251. [1](#)
- [4] A. Johnson, J. Montgomery, and L. Matthies, “Vision guided landing of an autonomous helicopter in hazardous terrain,” in *Proceedings of the 2005 IEEE International Conference on Robotics and Automation*, 2005, pp. 3966–3971. [1](#)
- [5] Bulent Ayhan, Chiman Kwan, Yool-Bin Um, and et al., “Semi-automated emergency landing site selection approach for uavs,” *IEEE Transactions on Aerospace and Electronic Systems*, vol. 55, no. 4, pp. 1892–1906, 2019. [1](#)
- [6] Eva König, Nicolai Voget, Max Hartmann, and Dieter Moormann, “Automatic identification of safety landing points for vtol uavs using geodata,” in *2025 International Conference on Unmanned Aircraft Systems*, 2025, pp. 1086–1093. [1](#)
- [7] Emre Saldiran, Mehmet Hasanzade, Aykut Cetin, and Gokhan Inalhan, “Ensuring operation time safety of vtol uav: Autonomous emergency landings in unknown terrain,” *IEEE Transactions on Aerospace and Electronic Systems*, vol. 61, no. 4, pp. 10694–10708, 2025. [1](#)
- [8] Jeonggeun Lim, Myeonggyun Kim, Hyungwook Yoo, and Jongho Lee, “Autonomous multirotor uav search and landing on safe spots based on combined semantic and depth information from an onboard camera and lidar,” *IEEE/ASME Transactions on Mechatronics*, vol. 29, no. 5, pp. 3960–3970, 2024. [1](#)
- [9] S. Scherer, L. Chamberlain, and S. Singh, “Autonomous landing at unprepared sites by a full-scale helicopter,” *Robotics and Autonomous Systems*, vol. 60, no. 12, pp. 1545–1562, 2012. [1](#)
- [10] Pedro F. Proen  a, Jeff Delaune, Rol, and Brockers, “Optimizing terrain mapping and landing site detection for autonomous uavs,” in *2022 International Conference on Robotics and Automation (ICRA)*, 2022, pp. 9668–9674. [1](#)
- [11] Yuan Hu, Jianlong Yuan, Congcong Wen, Xiaonan Lu, Yu Liu, and Xiang Li, “RSGPT: A remote sensing vision language model and benchmark,” *ISPRS Journal of Photogrammetry and Remote Sensing*, vol. 224, pp. 272–286, June 2025. [1](#)
- [12] Kartik Kuckreja, Muhammad S. Danish, and et al., “Geochat: Grounded large vision-language model for remote sensing,” *The IEEE/CVF Conference on Computer Vision and Pattern Recognition*, 2024. [1](#)
- [13] Wei Zhang, Miaoxin Cai, and Tong andet al. Zhang, “EarthGPT: A Universal Multimodal Large Language Model for Multisensor Image Comprehension in Remote Sensing Domain,” *IEEE Transactions on Geoscience and Remote Sensing*, vol. 62, pp. 1–20, 2024. [1](#)
- [14] Hengxing Cai, Jinhan Dong, Jingjun Tan, and et al., “Flightgpt: Towards generalizable and interpretable uav vision-and-language navigation with vision-language models,” *arXiv preprint arXiv:2505.12835*, 2025. [1](#)
- [15] Siwei Cai, Yuwei Wu, and Lifeng Zhou, “Llm-land: Large language models for context-aware drone landing,” 2025. [1](#)
- [16] Jarus, “Jarus guidelines on specific operations risk assessment (sora),” Tech. Rep., Joint Authorities for Rule-making on Unmanned Systems (JARUS): Cologne, Germany, 2019, Technical Report JAR-doc-06. [1](#)
- [17] Liang-Chieh Chen, Yukun Zhu, George Papandreou, Florian Schroff, and Hartwig Adam, “Encoder-Decoder with Atrous Separable Convolution for Semantic Image Segmentation,” in *ECCV*, vol. 11211, pp. 833–851. 2018. [2](#)
- [18] MMSegmentation Contributors, “MMSegmentation: OpenMMLab Semantic Segmentation Toolbox and Benchmark,” 2020. [2](#)
- [19] “2D Semantic Labeling Contest - Potsdam.” . [2](#)
- [20] Junjue Wang, Zhuo Zheng, Ailong Ma, Xiaoyan Lu, and Yanfei Zhong, “LoveDA: A Remote Sensing Land-Cover Dataset for Domain Adaptive Semantic Segmentation,” in *Proceedings of the Neural Information Processing Systems Track on Datasets and Benchmarks*, J. Vanschoren and S. Yeung, Eds., 2021, vol. 1. [4](#)